Jet amplification and cavity formation induced by penetrable fabrics in hydrophilic sphere entry

Daren A. Watson, Jeremy L. Stephen, and Andrew K. Dickerson

Citation: Physics of Fluids **30**, 082109 (2018); doi: 10.1063/1.5036655
View online: https://doi.org/10.1063/1.5036655
View Table of Contents: http://aip.scitation.org/toc/phf/30/8
Published by the American Institute of Physics

Jet amplification and cavity formation induced by penetrable fabrics in hydrophilic sphere entry

Daren A. Watson, Jeremy L. Stephen, and Andrew K. Dickerson[a)]
Department of Mechanical and Aerospace Engineering, University of Central Florida, Orlando, Florida 32816-2368, USA

(Received 17 April 2018; accepted 16 July 2018; published online 14 August 2018)

Studies of solid impact with fluid surfaces have traditionally considered splashing in the context of impactor shape and surface texture. However, it is not always possible to tune impactor properties for desired splash characteristics. In this experimental study, smooth, hydrophilic, free-falling spheres are allowed to impact a quiescent liquid surface for Weber numbers in the range of 400–1580. The liquid surface is modified by the inclusion of a thin fabric upon which a falling sphere strikes and penetrates at water entry. With respect to clean water, inclusion of a single layer of fabric on the surface increases the Worthington jet height across all entry speeds tested. As the sphere penetrates, the fabric is drawn inward, providing a fabric funnel through which a Worthington jet subsequently passes. We show that the presence of fabric increases the drag at entry and enables air-entraining cavities otherwise unattainable by hydrophilic spheres for the impact speeds tested. Such cavity formation is made possible by alteration of the flow separation angle, analogous to greater values of the advancing contact angle. *Published by AIP Publishing.* https://doi.org/10.1063/1.5036655

I. INTRODUCTION

Traditionally, splashing and splash reduction have been investigated in the context of impactor shape, speed, and wettability.[9,13,16,24] Such studies are applicable to military and naval applications such as missile water entry, space vehicle sea surface landing, and industrial processes.[18,21] In this study, we modify splashing characteristics without alteration of fluid or impactor properties but by the placement of thin layers of penetrable fabric upon the surface of a liquid pool.

Splash characteristics such as Worthington jets, air-entraining cavities, and radial splash crowns are dependent on surface tension, impactor wettability, and velocity.[3,9] The variance of these parameters for a desired splash outcome has been previously dubbed the "tuning of a splash."[19] Several studies modified surface tension and viscosity and showed that the jet height decreases with increasing viscosity, whereas the jet diameter is linearly proportional to the viscosity.[5,6,17,19] The splash height may also be tuned by changing the fluid depth, thereby influencing the amount of interaction of a collapsing cavity with the floor of a container.[19] When the impactor is a liquid droplet, the splash height reaches a maximum when the pool depth is roughly 2× the droplet diameter but attenuated when a sponge is affixed to the floor of the liquid pool.[19] Cavity pinch-off is delayed, and its shape is distorted by wall effects.[15] Pools deeper than cavities can be considered infinitely deep with respect to influencing splash mechanics. Here, we explore an alternate method for tuning a splash by altering fluid surface conditions in a deep pool.

Splash cavities have been extensively studied in the context of impactor shape,[13] wettability,[9] dynamics,[2,20,22,23] cavity shape,[24] and pinch-off location. The formation of an air-entraining cavity behind a solid impacting a liquid pool is greatly dependent on the hydrophobicity of the impactor.[2,9,10,25] Hydrophobic impactors repel water upon entry to create cavities at lower speeds than their hydrophilic counterparts. Water entry of hydrophilic spheres [Fig. 1(a)] at entry velocities $U \lessapprox 8$ m/s shows minimal displacement of the fluid and no cavity formation.[2,9] In this study, we consider the effect of a thin, penetrable fabric sitting atop a water surface on cavity formation.

Cavity forming splashes from spherical impactors typically include a well-developed dome rising above the surface whose periphery contains small jets that form an axisymmetric film.[4,10,11,19] This splash crown grows prior to the development of the primary jet due to the "under-pressure" and airflow behind the impactor. The maximum height attained by the splash crown is driven by inertial forces for Weber numbers We = $\rho U^2 D/\sigma \gg 1$, where ρ is the density of the fluid, D is the sphere diameter, and σ = 72 dyn/cm is the surface tension.[7] In our observations, the presence of a thin penetrable fabric inhibits the ascension of a typical splash crown.

This paper provides the first documented application of a thin penetrable fabric atop a deep liquid pool to alter splash characteristics of vertically impacting hydrophilic spheres. Splashing sequences with clean water using hydrophilic and hydrophobic spheres can be seen in Figs. 1(a) and 1(b), respectively. A cavity-forming impact induced by one layer of penetrable fabric can be seen in Fig. 1(c). Four layers of fabric are impenetrable by the impacting sphere in Fig. 1(d), producing no Worthington jet. In Sec. II, we present our experimental methods for impactor release and splash visualization. In Sec. III, we present results and theoretical considerations for the splash height, separation angle, and cavity

a)Author to whom correspondence should be addressed: dickerson@ucf.edu

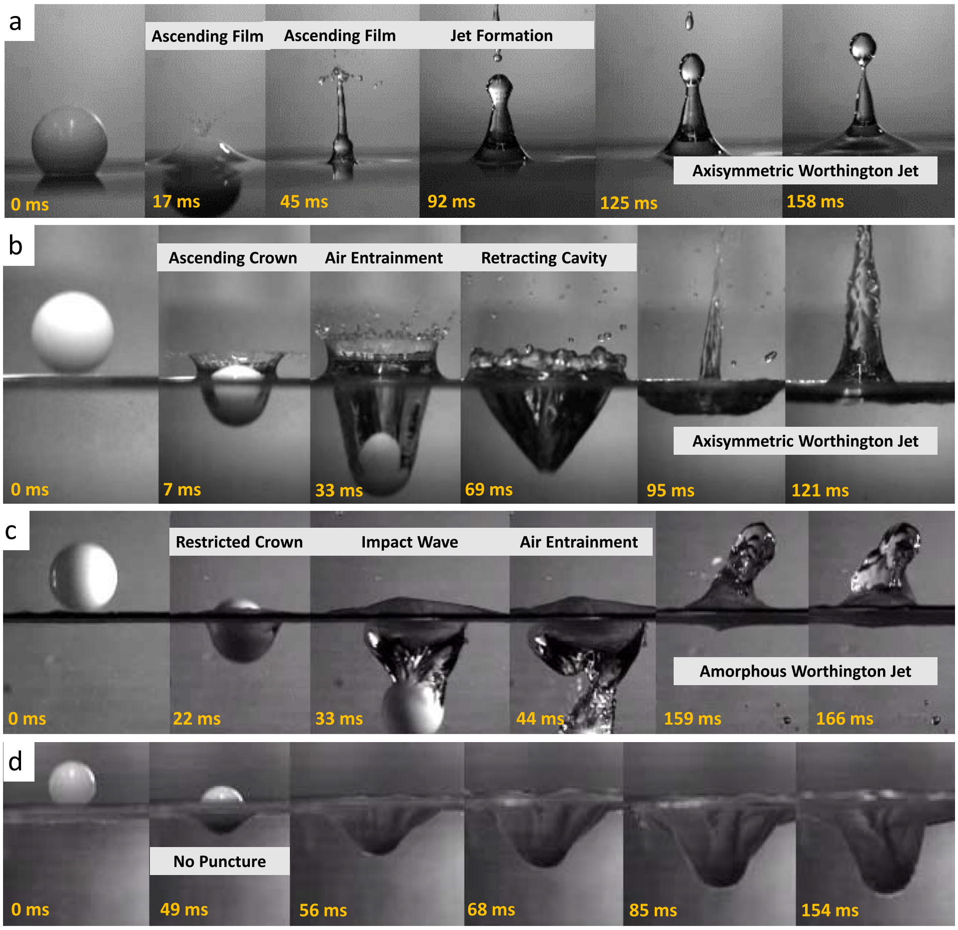

FIG. 1. Qualitative comparison of (a) hydrophilic and (b) hydrophobic sphere impacts on an unaltered surface. Penetrable, non-woven fabric alters entry dynamics of impacting hydrophilic spheres as seen by the inclusion of (c) one layer and (d) four layers of fabric. Spheres have an impact velocity of $U = 2.2$ m/s.

measurements for impacts in the range of Reynolds numbers $\mathrm{Re} = \rho DU/\mu = 17\,000$–$54\,000$ and $\mathrm{We} = 400$–1580, where $\mu = 8.90 \times 10^{-4}$ Pa s is the dynamic viscosity of water. These values are controlled by varying drop height $h = 11$–24 cm. In Sec. IV, we discuss the implications of this work and provide avenues for future research. In Sec. V, we draw conclusions from our results.

II. METHODS

A. Impact experiments

We conduct impact experiments using a 20×20 cm^2 aquarium and four smooth Delrin spheres of masses 2.07, 4.90, 7.68, and 11.51 g and diameters of 1.43, 1.90, 2.20, and 2.54 cm, respectively. The contact angles of water on Delrin, both equilibrium $\theta_e = 78°$ and advancing $\theta_a = 105°$, are measured photographically, using a syringe to deposit water onto the sphere's surface. The release mechanism consists of a hinged platform suspended over the liquid pool [Fig. 2(a)]. Elastic bands rapidly retract the platform such that the spheres' motion is purely vertical and irrotational and generates an impact velocity of $U \approx \sqrt{2gh}$, where $g = 9.81$ m/s^2 is the acceleration due to gravity. We clean and dry spheres with 99% isopropyl alcohol before each trial to preclude the influence of impurities and retrieve spheres from the pool with a sterile scoop.

For surface alteration, we use Georgia Pacific Compact coreless toilet paper with a compressed thickness of ~80 μm and comprised of chopped fibers 11 μm in diameter, shown in the SEM image of Fig. 2(b). We gently rest square plies ($\rho = 0.355$ g/cm^3, dry) atop the water such that the impacting sphere will strike the approximate center of the ply. The paper experiences volumetric absorption of water to remain neutrally buoyant during trials, and does not dissolve, breakup, or otherwise soil the water. Each drop condition is repeated at least 5 times to reduce the influence of experimental inconsistencies and water absorbed by the fabric replenished before each trial. The entire volume of the bath is replaced at least once daily.

We film impacts with a Photron Mini AX-100 high speed camera at 1000 fps using a 55 mm Nikkor lens [Fig. 2(a)]. In select trials, a Photron Mini UX-100 is added to the experiment to provide a top-down view of impacts on the fabric. We extract kinematic and geometric measurements from videos using Tracker, an open source analysis software. When reporting splash height H_{max}, we consider the tallest point of the coherent Worthington jet and not satellite droplets, as demonstrated in Figs. 2(c) and 2(d).

III. RESULTS

We impact a thin penetrable fabric atop the surface of a deep pool of water with four hydrophilic spheres from various heights and compare changes in the splashing dynamics with respect to an unaltered, clean surface. Spheres strike the center of a 10.5×10.5 cm^2 and tear through the fabric at sufficiently

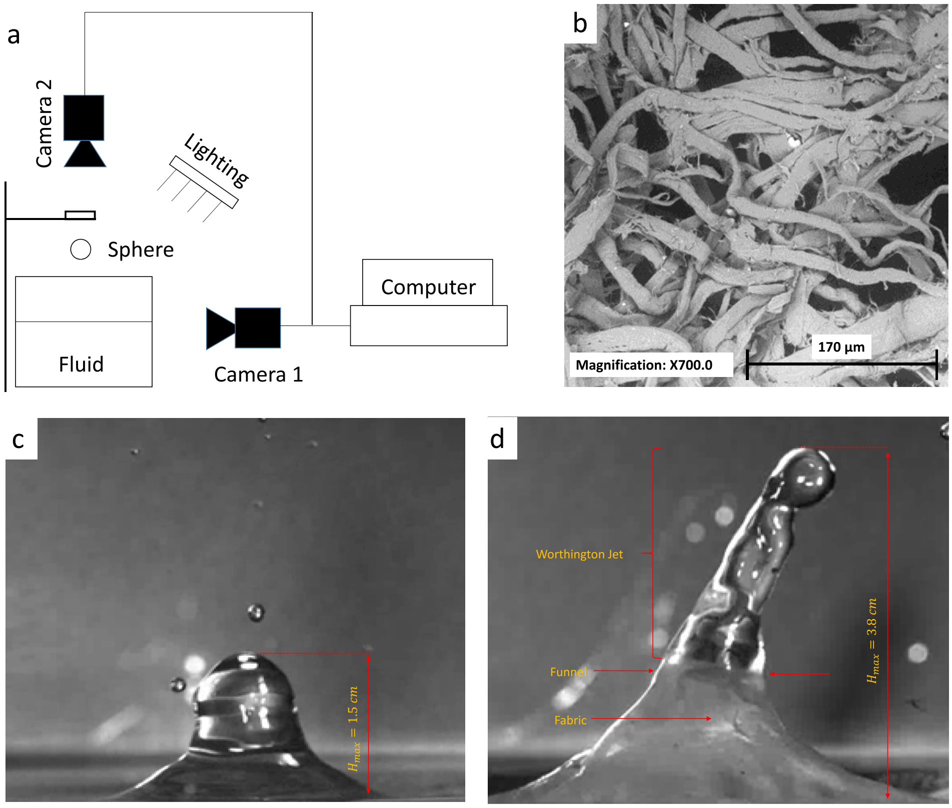

FIG. 2. (a) Experimental setup showing the Photron Mini AX-100 (Camera 1) for front views and the Photron Mini UX-100 (Camera 2) for overhead views. (b) SEM image of the non-woven fibers comprising the fabric used in experiments. Fibers have a width of approximately 11 μm. Impact outcomes for We = 716 on (c) an unaltered surface and (d) a surface with a single layer of non-woven fabric, where the fabric is drawn upward by the protruding jet.

high speeds. We observe that the presence of the fabric results in changes to the splash height, cavity formation, and splash crown.

A. Jet height control by layered fabric

We begin by measuring splash heights for hydrophilic spheres impacting clean water, as seen in Fig. 3(a). For the range of We = 400–1580 tested, we observe that splashes are on average amplified by the inclusion of a single ply, or layer, of fabric onto the splash domain and amplified by the inclusion of a double-layer of paper for We > 800. With three and four layers, the sphere does not penetrate the fabric for We < 1100 and We < 1500, respectively, and results in slower entry and no Worthington jet, represented by the points lying on the axis in Fig. 3(a). A plot of $H_{\max}/D$ vs. We is included in Fig. S1 of the supplementary material.

A pictorial comparison of the Worthington jet resulting from 0- and 1-ply of fabric for We = 716 is shown in Figs. 2(c) and 2(d). As expected with no fabric present, the hydrophilic Delrin sphere produces an axisymmetric Worthington jet and no cavity (Movie S1 of the supplementary material). With the inclusion of fabric, an air-entraining cavity follows the sphere,

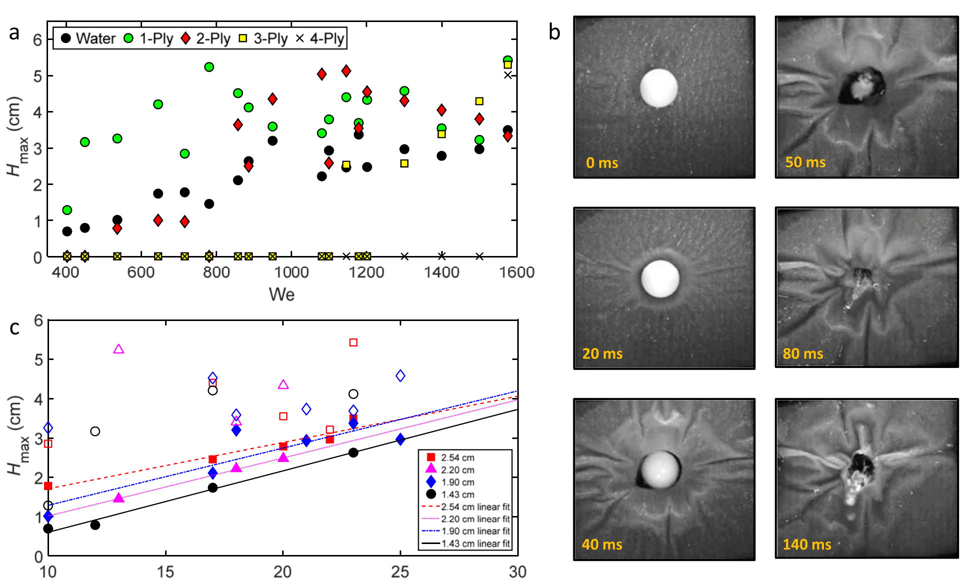

FIG. 3. (a) Worthington jet height H_{max} versus Weber number We. The number preceding "ply" denotes the layers of fabric. The presence of fabric creates greater jet heights for We sufficient to penetrate the fabric plies. (b) Time-sequence of a 2.54 cm sphere impact from an overhead view for We = 1580. (c) Worthington jet height $H_{\max}$ versus sphere release height h. Filled symbols denote impacts onto clean water, while open symbols denote impacts onto 1-ply of fabric. Linear fits are applied to clean water impacts only with R^2 = 0.931 (2.54 cm linear fit), 0.9984 (2.20 cm linear fit), 0.766 (1.90 cm linear fit), and 0.995 (1.43 cm linear fit). The presence of fabric disrupts a linear progression of splash height, with $R^2 < 0.65$ for all spheres.

so long as the sphere penetrates the fabric (Movie S2 of the supplementary material). As the cavity retracts, the jet propagates through the hole torn in the fabric by the passing sphere, as seen in Figs. 2(d) and 3(b), resulting in amorphous jets (Movie S3 of the supplementary material) that are narrower for higher numbers of fabric plies. In some cases, this action results in greater jet heights, as evidenced by the rightmost points of Fig. 3(a).

As seen in Fig. 3(a), splash height increases with We. For the range of Re = 17 000–54 000 tested, inertial effects dominate viscous effects for impacts in the absence of fabric. In the limit of an inviscid fluid, the kinetic energy of the impacting sphere $E_{k,s} = \rho_s V_s g h$ will be converted to potential energy of the jet $E_{p,j} = \rho g V_j H_{max}$, where ρ_s and V_s are the density and volume of the sphere, respectively, and V_j is the volume of the jet. Accordingly,

$$\rho_s V_s g h \sim \rho V_j g H_{max}. \tag{1}$$

Although not tested, we expect that $V_j \sim V_s$. When a hydrophilic sphere strikes the fluid, an ascension film spans the diameter, as seen in Fig. 1(a). With this assumption and noting that ρ_s/ρ = constant in our experiments, Eq. (1) becomes

$$H_{max} \sim h. \tag{2}$$

The linear relationship predicted by Eq. (2) is confirmed by the filled points in Fig. 3(c) for impacts onto clean water. We find disruption of this linear trend by the addition of fabric.

B. Artificial increase in water repellency

The application of the thin fabric atop the water surface not only amplifies the jet height with respect to hydrophilic impactors on clean water but also facilitates the formation of an air-entraining cavity (Movie S4 of the supplementary material). The fabric alters separation characteristics (angle Θ and location ϕ), as defined in Fig. 4(a), due to prevention of

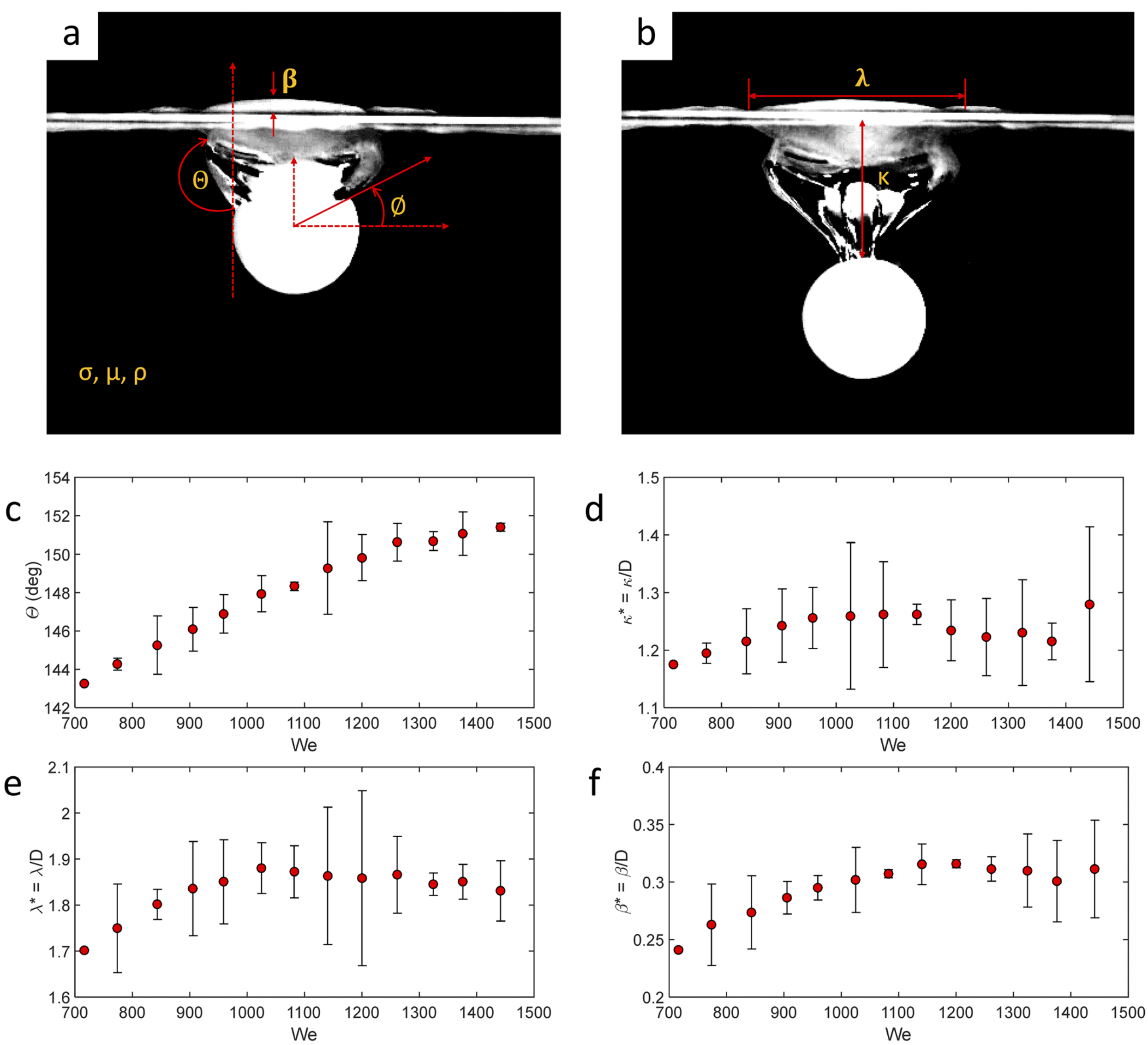

FIG. 4. Diagrams depicting (a) the separation angle Θ, separation location ϕ, and impact wave height β, and (b) cavity width λ and depth κ for a cone-shaped quasi-static seal. Θ is measured from the location of flow separation ϕ, and β is measured from the free surface. The relation between the Weber number and the (c) separation angle Θ, (d) cavity depth κ, (e) cavity width λ, and (f) impact wave height β. Properties are non-dimensionalized in terms of the sphere diameter, D = 2.20 cm.

the ascending film seen in Fig. 1(a) such that the water cannot flow toward the top of the sphere. The resulting flow separation is characteristically similar to impactors that have greater advancing contact angles,[9] θ_a, inducing separation through hydrophobicity alone.

We vary the drop height and observe the punctured fabric acting as a barrier between the sphere and fluid as subsurface cavities develop. An increase in this separation angle Θ from a low of 143°, We = 716, to a high of 151°, We = 1441, can be seen in Fig. 4(c) using a sphere of fixed $D = 2.20$ cm and 1-ply of fabric. The increase in Θ with U indicates that the impactor produces steeper cavity walls, overcoming the tensile influences of the fabric with greater momentum values. Cavities formed by this process are characterized as quasi-static seals as pinch-off occurs at or near the sphere.[1,24] After about 60 ms, the sphere exits the cavity which retracts, leading to the formation of the primary Worthington jet.

Across the range of experimental We, we find dimensions of cavities created by a sphere of fixed $D = 2.20$ cm and 1-ply of fabric shows little variation. The non-dimensional cavity depth $\kappa^* = \kappa/D$ increases by less than 8%, and the non-dimensional cavity diameter $\lambda^* = \lambda/D$ increases by less than 15% with increasing We, as seen in Figs. 4(d)–4(f). The existence of an impact wave [Fig. 1(d)] is a result of the inhibition of a splash crown by the fabric. We likewise measure little change in the non-dimensional impact wave height $\beta^* = \beta/D$ as We increases. The weak dependence of the cavity size to U is rationalized by noting that after the sphere ends contact with the fabric, its hydrophilic nature prevails such that the sphere is no longer able to propagate the cavity further. Therefore, we posit that cavity properties are only a strong function of sphere size. For an unaltered surface, a cavity forming impact must exceed a critical velocity U_c given by[9]

$$U_c = \begin{cases} \varepsilon\sigma/\mu & \text{if } \theta_a \le 90^\circ \\ \psi\sigma[\pi - \theta_a]^3/9\mu & \text{if } \theta_a \ge 90^\circ \end{cases}, \tag{3}$$

where $\varepsilon = 0.1$ and $\psi = 7/30$ are numerical pre-factors set to match previous results.[9] The solid curve in Fig. 5 represents the value of U_c for unaltered surface conditions and corresponds to 8.1 m/s, We = 23 763, for $\theta_a \le 90^\circ$ and $\mu = 0.89$ cP. The onset of cavity formation[9,24] for spherical impactors can be accomplished by an increase in either θ_a or μ. For the case of fabric placement onto the impact plane, we have an increase in the separation angle, which has the same dynamical effects as an increase in θ_a which provokes cavity formation over the range of U on test.

The circle in Fig. 5 shows the impacting Delrin sphere firmly outside the cavity-forming region, consistent with our experiments with 0-ply. This sphere can be found inside the cavity-forming region by conservatively setting $\theta_a = \Theta$ as denoted by the square in Fig. 5, the result of impacting 1-ply of fabric. We note that in trials with a hydrophobic sphere with $\theta_a = 135^\circ \pm 3^\circ$ impacting clean water (0-ply), the separation angle is $\Theta = 168^\circ \pm 1^\circ$, N = 6.

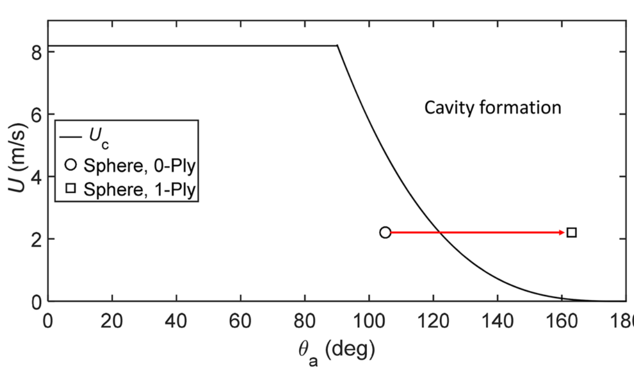

FIG. 5. Threshold velocity for cavity formation as a function of the advancing contact angle. For impacts onto clean water, spheres can be found in the non-cavity forming region. The introduction of fabric increases the separation angle, comparable to increasing θ_a, thereby shifting impacts into the cavity-forming region.

C. Fabric increases drag force at fluid entry

The presence of penetrable fabric plies increases drag force at entry. We determine the additional drag force from the addition of fabric layers by tracking the position of a 2.54 cm diameter sphere released from 24 cm as it impacts the liquid/fabric interface, as seen in Fig. 6(a). A force balance for a sphere of mass m falling vertically into a quiescent liquid bath is given by

$$(m + m_a)a = mg - F_b - F_d, \tag{4}$$

where a is the acceleration of the sphere. The buoyant force due to hydrostatic pressure $F_b = \rho g\left(\frac{\pi}{12}D^3 + A(y)y\right)$, where y is the coordinate into the fluid depth and $A(y)$ is the wetted area of the sphere entering the bath. This form of buoyant force follows conventions established in previous work[2] and assumes that the cavity adjoins the equator for simplicity. For

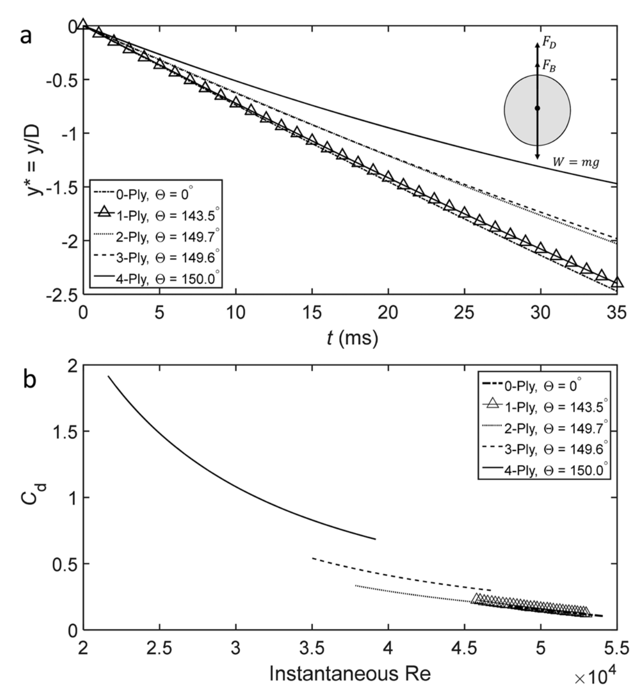

FIG. 6. (a) Temporal tracks of the vertical position for impacting spheres with 0- to 4-layers of fabric atop the water. Trajectories are non-dimensionalized in terms of the sphere diameter, $D = 2.54$ cm. (b) Relation between the coefficient of drag C_d and the Reynolds number Re for impacting spheres with 0- to 4-layers of fabric atop the water. Addition of fabric increases drag on impacting spheres.

further simplification, we treat buoyant force as constant such that

$$F_{\mathrm{b}} = \rho g \pi \left(\frac{D^3}{12} + \frac{D^2}{4} \frac{\kappa}{2} \right), \tag{5}$$

where we treat $\kappa = D$ according to Fig. 4(d). In our experiment and model, we consider only the period of time the sphere is interacting with the fabric and maintains an air-entraining cavity. Drag force[2,8,14] is given by $F_{\mathrm{d}} = \frac{\pi}{8} \rho D^2 C_{\mathrm{d}} u^2$, where C_{d} is the drag coefficient and $u = u(t)$ is the time-varying velocity. The effect of accelerating fluid by the falling sphere is accounted for by the added mass $m_a = \frac{\pi}{6} \rho D^3 C_{\mathrm{m}}$, where $C_{\mathrm{m}} = 0.5$ is the added mass coefficient, treated as constant[2,23] across all cases. It is noteworthy that our model is not sensitive[2] to the value of C_{m}. Equation (4) can be rewritten as

$$m' a = mg - \frac{5}{24} \rho g \pi D^3 - \frac{1}{8} \rho \pi D^2 C_{\mathrm{d}} u^2, \tag{6}$$

where $m' = m + m_a$. We transform Eq. (6) into a first order non-linear differential equation. Accordingly,

$$\frac{\mathrm{d}u}{\mathrm{d}t} = \frac{mg}{m'} - \frac{\rho g \pi D^2}{8m'} \left(\frac{5}{3} D + \frac{C_{\mathrm{d}}}{g} u^2 \right). \tag{7}$$

We smooth position track data with a Savitzky-Golay filter[12] [Fig. 6(a)] to remove the effects of experimental error prior to numerical differentiation. The resulting velocity curves, $u(t)$, are again smoothed prior to a second and final numerical differentiation, providing $\mathrm{d}u/\mathrm{d}t$. Using Eq. (7), we solve for values of C_{d}, which are plotted against instantaneous Re in Fig. 6(b). Greater numbers of fabric plies slow the sphere's motion more rapidly and result in greater values of C_{d}.

The average values of $C_{\mathrm{d}} = 0.14$, 0.17, 0.26, 0.40, and 1.15 for 0-, 1-, 2-, 3-, and 4-plies, respectively. By treating C_{d} as constant throughout the duration of impact, we can solve for an equivalent change in the sphere diameter D_{d}, increasing form drag, which corresponds to each impact scenario. We include a plot of a non-dimensionalized form drag diameter $D^* = D_d/D$ vs. instantaneous Re in Fig. S3 of the supplementary material.

IV. DISCUSSION

Our study shows that vertical impacts by hydrophilic spheres on a thin fabric placed atop a deep pool of water experience amplified jet heights and cavity formation, as compared with pure water. In our observations, these behaviors exist only when spheres penetrate the fabric. Those impacts which do not penetrate fabric sit on the axis in Fig. 3(a) and do not achieve a sufficient impact momentum to create a cavity. For these non-penetrating impacts, the theoretical considerations discussed in Sec. III B do not apply. We expect the reaction of spheres to 3- and 4-plies of fabric at We < 1500 is qualitatively similar to using any thickness of woven fabric, which would maintain its tensile integrity when wet.

When using fabric to allay splash-back, it is imperative that falling objects are unable to puncture the fabric, either by excessive layering or by sufficient tensile strength. Though we made no attempt to customize the height of Worthington jets, careful selection of fabric may enable tunable jet height with this method. However, as evidenced by Fig. 3(c), it is unknown how fabric properties affect splashing dynamics. We rationalize disruption to our splash height scaling prediction of Eq. (2) by the unpredictable nature of energy dissipation imposed by fabric at impact. The spheres' kinetic energy is converted to tearing and mobilizing the fabric and creating a cavity [Fig. 3(b)].

The ability to continue to draw inward after sphere passes enables the narrowing of the Worthington jet. A sheet of fabric which has a much greater area will possess sufficient inertia to prohibit mobilization toward the puncture, while a sheet approaching the diameter of the sphere will have insufficient material to remain wider than λ. In either case, we expect wider jets. Likewise, in cases where a fluid surface coating is stiff and cannot retract toward a puncture, if the surface is covered by a thin sheet of ice, for example, we expect wider jets. The sensitivity of jet characteristics to the fabric size and mobility is therefore an area requiring further investigation.

Fabrics which are functionally impenetrable by impacting spheres but impacted at higher We than reported in Fig. 3(a) form cavities and splash, as seen in Movie S5 of the supplementary material. In these cases, the falling sphere will have sufficient momentum to fully submerge a fabric sheet. In doing so, the edges of the sheet generate the most dominant splashing feature. The properties of fabric and sphere for such a transition from non-splashing to splashing are an avenue of further study. In this study, we were not concerned with fabric elasticity, which will likewise affect impact dynamics and fabric puncture. Accordingly, the transition between a penetrated and intact fabric, and how this transition is related to fabric strength, elasticity, and sphere dynamics, is a topic of future consideration.

Fabric sheets with pre-cut holes larger than the impacting sphere allow passage as if not present, producing splash characteristic to that seen in Fig. 1(a), so long as the sphere does not contact any portion of the fabric at entry. We provide an example in Movie S6 of the supplementary material with a precut circle with diameter $3D/2$. In this case, there is no evident mobilization of the fabric. In the case where the precut is smaller than the sphere diameter, interaction with the fabric produces a cavity at entry, similar to the impact depicted in Fig. 1(c). We provide an example of such an impact in Movie S7 of the supplementary material, where the precut hole has diameter $D/2$.

V. CONCLUSION

Here we have shown hydrophilic spheres impacting a thin layer of penetrable fabric atop a water bath experience Worthington jet height amplification and air-entraining cavities for Weber numbers 400–1580 with respect to impacts on clean water. We layer the fabric from 1- to 4-plies which creates greater drag on spheres at entry and induces flow separation, creating a cavity. Punctured fabric draws inward as an air-entraining cavity is formed, providing a constricted opening through which the protruding Worthington jet issues. With a growing number of plies, spheres must impact at greater Weber numbers to puncture the fabric. Those impacts that leave fabric intact do not create cavities or Worthington jets and are effective at splash mitigation. The use of a single layer of fabric, which is easily penetrated, allows hydrophilic spheres to form cavities at minute entry velocities. Across the range of entry velocities tested, separation angles for single layers increase with increasing velocity, whereas cavity geometry exhibits no strong correlation.

SUPPLEMENTARY MATERIAL

See supplementary material for 7 movies and a supplementary document. The document contains descriptions of the movies and additional plots for non-dimensionalized jet height $H_{\max}/D$ vs. We, non-dimensionalized puncture area α^* vs. We, and non-dimensionalized form drag diameter D^* vs. instantaneous Re.

ACKNOWLEDGMENTS

We would like to acknowledge Dr. Tadd Truscott for valuable feedback, the College of Engineering and Computer Sciences (CECS) at the University of Central Florida for funding this project, and Hiba Khan and Nicholas Smith for assisting us with our experiments.

[1] Aristoff, J. and Bush, J., "Water entry of small hydrophobic spheres," J. Fluid Mech. **619**, 45–78 (2009).
[2] Aristoff, J., Truscott, T., Techet, A., and Bush, J., "The water entry of decelerating spheres," Phys. Fluids **22**, 032102 (2010).
[3] Beczek, M., Ryzak, M., Sochan, A., Mazur, R., Polakowski, C., and Bieganowski, A., "The differences in crown formation during the splash on the thin water layers formed on the saturated soil surface and model surface," PLoS One **12**, e0181974 (2017).
[4] Cai, Y. K., "Phenomena of a liquid drop falling to a liquid surface," Exp. Fluids **7**, 388–394 (1989).
[5] Castillo-Orozco, E., Davanlou, A., Choudhury, K. P., and Kumar, R., "Droplet impact on deep liquid pools: Rayleigh jet to formation of secondary droplets," Phys. Rev. E **92**, 053022 (2015).
[6] Cheny, J. and Walters, K., "Extravagant viscoelastic effects in the Worthington jet experiment," Papers Presented at the *Workshop on Unresolved Experimental Dilemmas in the Dynamics of Complex Fluids* [J. Non-Newtonian Fluid Mech. **67**, 125–135 (1996)].
[7] Cossali, G. E., Marengo, M., Coghe, A., and Zhdanov, S., "The role of time in single drop splash on thin film," Exp. Fluids **36**, 888–900 (2004).
[8] Cross, R., "Vertical impact of a sphere falling into water," Phys. Teach. **54**, 153–155 (2016).
[9] Duez, C., Ybert, C., Clanet, C., and Bocquet, L., "Making a splash with water repellency," Nat. Phys. **3**, 180–183 (2007).
[10] Gekle, S. and Gordillo, J. M., "Generation and breakup of Worthington jets after cavity collapse. Part I. Jet formation," J. Fluid Mech. **663**, 293–330 (2010).
[11] Gilbarg, D. and Anderson, R. A., "Influence of atmospheric pressure on the phenomena accompanying the entry of spheres into water," J. Appl. Phys. **19**, 127–139 (1948).
[12] Krishnan, S. R. and Seelamantula, C. S., "On the selection of optimum Savitzky-Golay filters," IEEE Trans. Signal Process. **61**, 380–391 (2013).
[13] Kubota, Y. and Mochizuki, O., "Influence of head shape of solid body plunging into water on splash formation," J. Visualization **14**, 111–119 (2011).
[14] Lee, M., Longoria, R., and Wilson, D., "Cavity dynamics in high-speed water entry," Phys. Fluids **9**, 540–550 (1997).
[15] Mansoor, M. M., Marston, J. O., Vakarelski, I. U., and Thoroddsen, S. T., "Water entry without surface seal: Extended cavity formation," J. Fluid Mech. **743**, 295–326 (2014).
[16] Marston, J. O., Truscott, T. T., Speirs, N. B., Mansoor, M. M., and Thoroddsen, S. T., "Crown sealing and buckling instability during water entry of spheres," J. Fluid Mech. **794**, 506–529 (2016).
[17] Ogawa, A., Utsuno, K., Mutou, M., Kouzen, S., Shimotake, Y., and Satou, Y., "Morphological study of cavity and Worthington jet formations for Newtonian and non-Newtonian liquids," Part. Sci. Technol. **24**, 181–225 (2006).
[18] Shi, H., Itoh, M., and Takami, T., "Optical observation of the supercavitation induced by high-speed water entry," J. Fluids Eng. **122**, 806–810 (2000).
[19] Shin, J. and McMahon, T. A., "The tuning of a splash," Phys. Fluids A **2**, 1312–1317 (1990).
[20] Techet, A. and Truscott, T., "Water entry of spinning hydrophobic and hydrophilic spheres," J. Fluids Struct. **27**, 716–726 (2011).
[21] Thoroddsen, S. T., Etoh, T. G., Takehara, K., and Takano, Y., "Impact jetting by a solid sphere," J. Fluid Mech. **499**, 139–148 (2004).
[22] Truscott, T. and Techet, A., "Water entry of spinning spheres," J. Fluid Mech. **625**, 135–165 (2009).
[23] Truscott, T., Epps, B., and Techet, A., "Unsteady forces on spheres during free-surface water entry," J. Fluid Mech. **704**, 173–210 (2012).
[24] Truscott, T. T., Epps, B. P., and Belden, J., "Water entry of projectiles," Annu. Rev. Fluid Mech. **46**, 355–378 (2013).
[25] Zhao, S., Wei, C., and Cong, W., "Numerical investigation of water entry of half hydrophilic and half hydrophobic spheres," Math. Probl. Eng. **2016**, 1–15.